Fifth International Symposium on Marine Propulsion
smp'17, Espoo, Finland, June 2017

Dynamic Instabilities in Propeller Crashback

Matthew Pontarelli, J. Ezequiel Martin, Pablo M. Carrica

IIHR-Hydroscience and Engineering, The University of Iowa, Iowa City, IA

ABSTRACT

Propeller crashback generates flow instabilities which can cause large lateral forces. These forces induce moments that increase the difficulty in controlling vessel motion. During a full crashback stopping maneuver from operating speed, the vessel will transition from high advance coefficients (J), greater than or equal to -1.0, to advance coefficients approaching zero, as vessel speed is arrested while propeller speed is maintained. High resolution computational fluid dynamics (CFD) simulations through this range of advance coefficients were performed for two propellers to obtain open water curves (OWC) in the crashback quadrant. Different flow regimes are described, as characterized by the dynamics of the resulting ring vortex created by the opposite flows of the free stream and the induced flow of the propeller. Results from a crashback maneuver for a submarine are also discussed.

Keywords

Crashback operation; Computational Fluid Dynamics; Flow Instabilities.

1 INTRODUCTION

Crashback operation generates large concentrated loads near the propeller tips, resulting in severe loading of the propeller roots. This is of fundamental importance, regarding the integrity of the propeller, and a main focus of interest in the evaluation of crashback conditions. Also of importance is the fact that a propeller operating in crashback creates instabilities in the flow field near the rotor which can cause large in-plane (lateral) forces. These forces can induce non-negligible, undesirable motions and affect controllability of the vessel. It is expected that large lateral motions occur during a crashback maneuver as a positive feedback process between the lateral displacement and forces. However, it has been shown (Jiang et al., 1996) that large lateral forces can occur even when yawing of the system is restricted, such as during open water or water tunnel tests. It has been well documented that the flow around the propeller develops unsteady, asymmetric ring vortices (Jiang et al., 1996; Jessup et al., 2004) for certain operational conditions that result in important radial flows near the propeller and are considered responsible for the persistent lateral forces. The objective of this work is to characterize the flow instabilities resulting in those persistent in-plane forces.

Previous numerical computations of crashback conditions using unsteady Reynolds-averaged Navier-Stokes (URANS) methodology have limited success in describing the observed flow, and Large Eddy Simulation (LES) approach has been preferred to describe this massively separated flows (Jang and Mahesh, 2013). Hybrid methods, such as Delayed Detached Eddy Simulation (DDES), as used in this work, provide a successful alternative to LES, with good agreement with available data both in the mean and fluctuating characteristics of the flow.

2 METHODOLOGY

2.1 REX

Computations were performed with the naval hydrodynamics solver REX using a shear stress transport (SST)-based DDES approach. REX is a multi-grid structured URANS solver developed at The University of Iowa. Many capabilities required for naval and other engineering applications such as multibody dynamics, including arbitrarily large motions, free surface and two phase modeling, implementation of controllers and coupling with third-party solvers for components simulations are available in REX. Turbulence modeling uses a blended $k-\varepsilon / k-\omega$ model (Menter, 1994) for the RANS approach, both with no-slip conditions at solid walls, or using wall functions. Additionally, several hybrid RANS/DES models are included to improve the resolution of flow structures away from surfaces, without incurring in the demanding discretization requirements of true LES models. Further details on REX can be found in Li et al. (2015) and the literature therein.

2.2 Geometry, Grids and Simulation Conditions

Two different geometries were considered. DTMB 4381 is a right-handed five-bladed propeller with no rake or skew and a diameter of 0.305 m; MARIN 7371 R is six bladed stock propeller with diameter of 0.273 m. Experimental data for open water (towing tank) and water tunnel operation in crashback for 4381 is available in Hecker and Remmers (1971) and Chesnakas et al. (2004), respectively; a crashback maneuver for the Joubert BB2 free running

model of a submarine fitted with 7371R is reported in Carrica et. al. (2016).

The domain for open water calculations is discretized using multiblock/overset structured grids, with pre-calculated connectivity interpolation coefficients between grids, which are then rotated rigidly to impose the propeller motion. Blades, hub and shaft geometries are described using body-fitted curvilinear grids. The grid system includes a large cylindrical background grid surrounding a Cartesian grid with block to block boundary conditions at their interface. The total number of grid points for propeller 4381 is 22.2M, and 18.4M for 7371 R. A set of one coarser and finer grids was used for 7371R to check grid convergence, but those results are not presented herein. Boundary conditions are applied to both the Cartesian and cylindrical background grids. The cylindrical "sleeve" grid (Figure 1) was used to prevent fluxes at the corners of the Cartesian background grid and extend the overall domain. A wide domain was necessary to prevent the pressure field created by crashback flow interacting with the far-field boundary conditions in the computation.

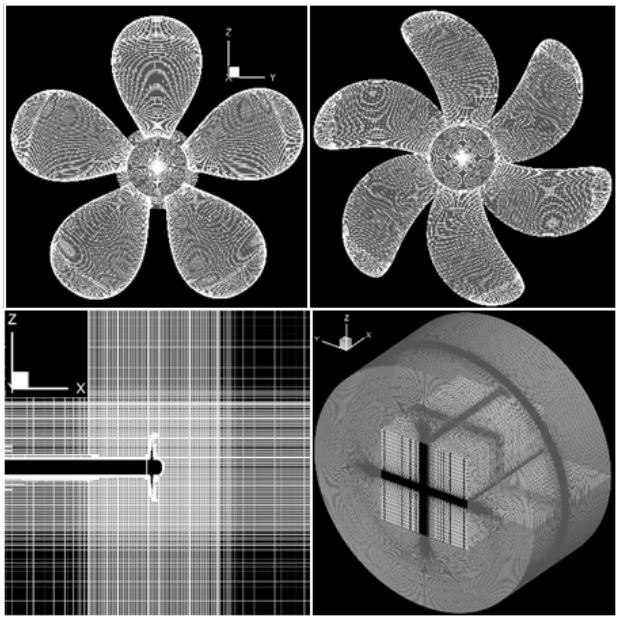

Figure 1: Clockwise from top left: surface grids for DTMB 4381 & MARIN 7371R; Background grid; Refinement grid.

All open water simulations were computed using a propeller rotation of 1 degree per time step. The different advance ratios $J = U/nD$, with U the free-stream velocity and D the propeller diameter, were obtained by modifying the inlet velocity. A constant rotational speed of 15 rps was used for 7371R, and for 4381it was modified as reported in Chesnakas et al. (2004) and Chang et al. (2008). Reynolds numbers were matched to experimental conditions of Chesnakas et al. (2004) for 4381 and those of 7371R in straight ahead operation. Results for free running Joubert BB2 are only presented herein in the context of the crashback maneuver and the reader is referred to Carrica et al. (2016) for details on the setup of those simulations.

3 RESULTS AND DISCUSSION

3.1 Validation - OWC

3.1.1 Straight Ahead Operation

Straight ahead simulations were run for the 4381 and 7371R propellers, see Figure 2 (top). Simulations for both propellers compared well with experimental data. In general, thrust was slightly under predicted while torque was over predicted. Straight ahead data is the only available open water dataset for 7371R, therefore these results are included to support the validation of the numerical runs for this propeller.

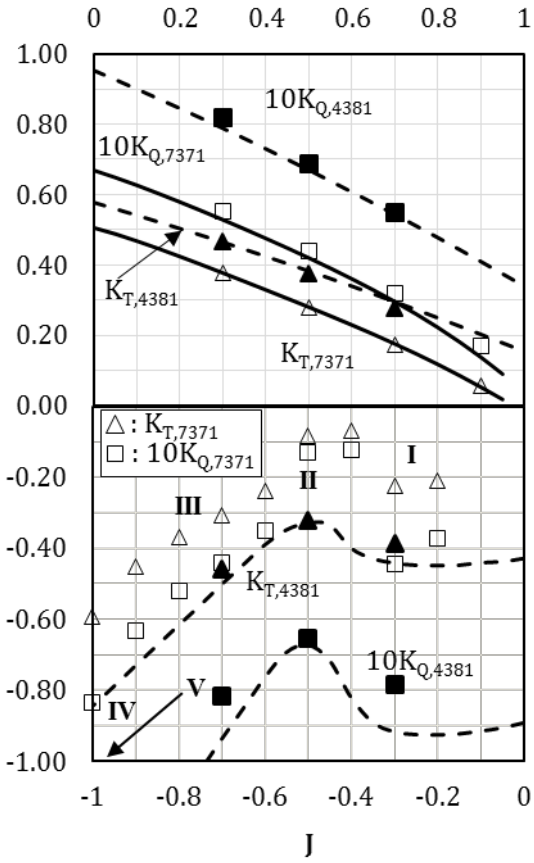

Figure 2: Forward (top) and crashback (bottom) open water curves for DTMB 4381 (open symbols) and MARIN 7371R propellers (solid). Available experimental data is shown as continuous and dashed lines. Flow regimes I through V are identified in crashback curve.

3.1.2 Crashback Operation

Validation cases were run using the 4381 geometry for J = -0.3, -0.5, and -0.7 (Fig. 2, bottom). These advance coefficients were chosen since they produce the three main flow regimes observed. The thrust and torque coefficients $K_T = T/(\rho n^2 D^4)$ and $K_Q = Q/(\rho n^2 D^5)$ with T thrust, Q torque and ρ density, compare well to the experimental open water data (Hecker and Remmers, 1971). Large uncertainties for average thrust and torque were reported from other experimental investigations for 4381 in a variable pressure water tunnel (Chesnakas et al., 2004). It is believed that the difference when comparing tow tank and water tunnel results is due mostly to wall confinement effects.

3.2 Flow analysis for 7371R in crashback

Different flow regimes were identified in Figure 2 for the crashback curve of 7371R. Similar regimes were also identified for 4381. Figure 3 illustrates the flow field at representative advance coefficients for each regime. Given the opposite directions of the free stream and the propeller induced flow, a recirculation occurs in all cases, as shown in the lower panel of Figure 3. This recirculation appears as a ring vortex that migrates from an upstream location at low J to a downstream position for large J. The strength and behavior of the vortex is strongly dependent on its location, and for sufficiently low or high J values (regimes I and V), can be only observed in the average velocity field. As J approaches zero (regime I), a second ring vortex is also observed. For intermediate J a persistent vortex structure is observed in the instantaneous flow as well, first as a symmetric attached ring vortex near the blade tips (region II), then as a rotating asymmetric but persistent ring (III), and finally as a periodically shedding structure (IV). At moderate advance coefficients greater than -0.5 but less than -1.0 (regime III), the ring vortex moves downstream of the propeller plane, but a section of the vortex maintains its proximity to the blades, creating an asymmetry in the ring vortex. Furthermore, the interaction with the blades imposes a rotation of the ring vortex that revolves around the propeller axis at a very low frequency and against the rotation direction of the propeller. The origin of this precession speed is still being investigated, as it does not appear to be dictated by the propeller wake swirl, which remains co-rotating with the propeller at all advance ratios. The rest of the ring vortex is pushed away from the propeller plane and wanders around the radial and axial directions. The area in which the ring vortex wanders is clearly identified by the mean flow streamlines, shown in Figure 3 for J = -0.7. Similar asymmetry, rotation and wandering was observed by Bridges et al. (2008) for dynamic advance coefficient experiments for 4381. As J continues to decrease, the strong ring vortex is broken down by the freestream flow as the ingestion of the propeller is not strong enough to maintain the ring vortex attached, resulting in periodic shedding of the vortex. At advance coefficients greater than -1.0, the propeller introduces random vortical structures to the flow, which are transported downstream by the higher velocity freestream flow.

Phase-averaged quantities (Figure 4 and 5) also support the previous description of the flow. At low advance ratios the flow is mostly symmetric; however notice for J = -0.3 that small variations on the velocity near the blade tip persist even after averaging. The presence of two vortex rings is clearly seen in Figure 5; notice that the observed discontinuities are due to the larger variability for the upstream vortex, compared to the one closest to the propeller. The attached ring vortex is clearly observed for J = -0.5 and circumferential variability is at a minimum. As a rotating asymmetric ring vortex appears for J = -0.7, the phase-averaged flow field shows little resemblance to the instantaneous flow. A better representation of the flow is achieved using the slow rotational speed of the vortex ring (about 1/18 of the propeller rotational speed), as shown in

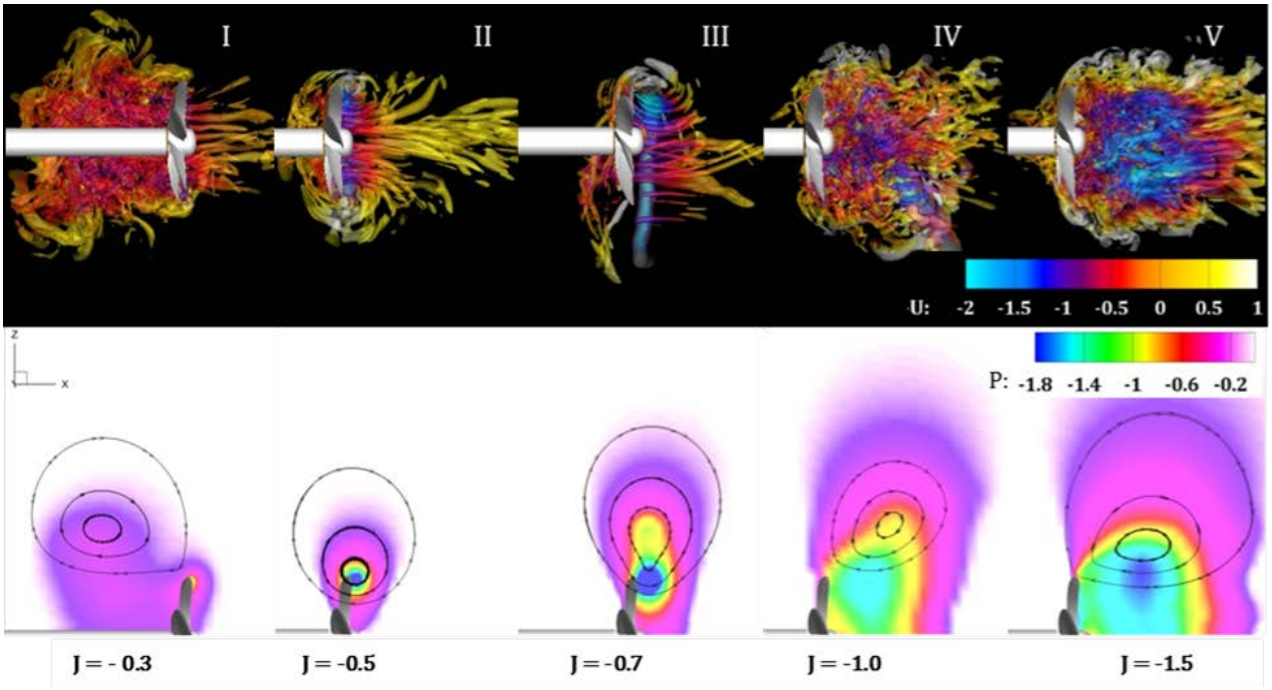

Figure 3 Top: Instantaneous flow field for 7371R, with turbulent structures colored by non-dimensional axial velocity, port view; Bottom: Phase- and circumferential averaged pressure with streamlines, port view. Advance coefficients, and flow regime as identified in the open water curve, are detailed for all cases.

the lowest panels of Figure 4 and Figure 5. The rotation of the vortex in opposite direction to the propeller can be inferred from the location of the reattachment point, where the transitional region between the free stream and the flow through the propeller becomes thinner, as the ring vortex grows in strength (compared to the apparent direction of rotation for the standard phase-average); alternatively, in Figure 5 the reattachment point is marked by a twist of the vortex, in the otherwise smooth surface. Notice that the presence of the ring vortex affects the velocity distribution over the entire propeller, resulting in non-uniform force distribution on the blades.

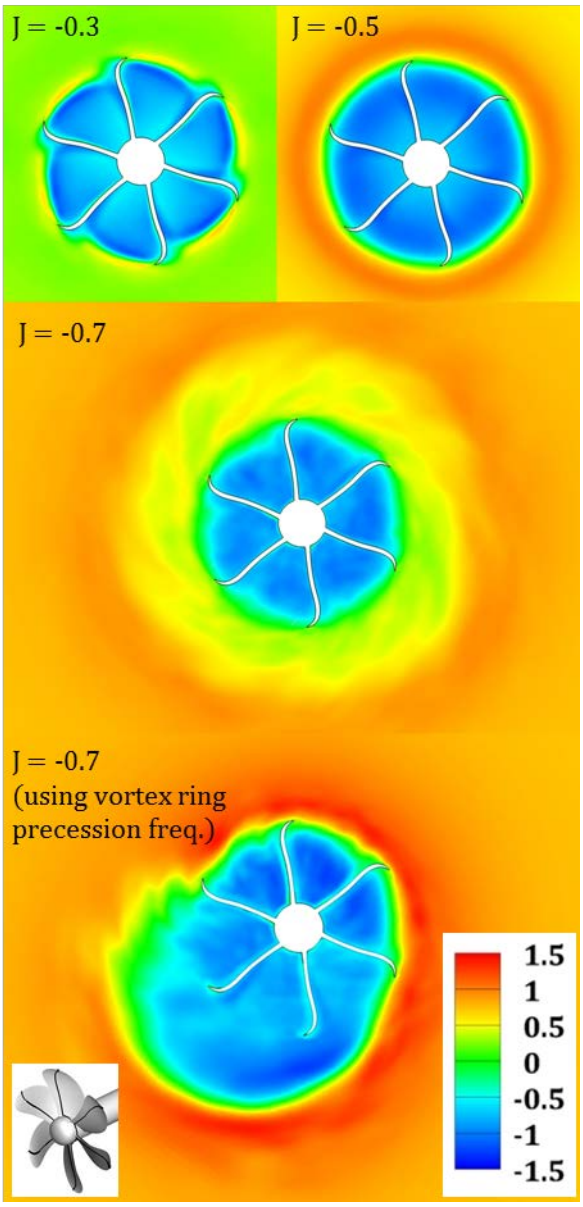

Figure 4: Phase-averaged longitudinal velocity. The propeller rotational speed is used for averaging, except for bottom panel for which the rotational frequency of the vortex ring around the axial direction is used. The cross sections shown correspond approximately to the center plane of the propeller, as depicted in the inset.

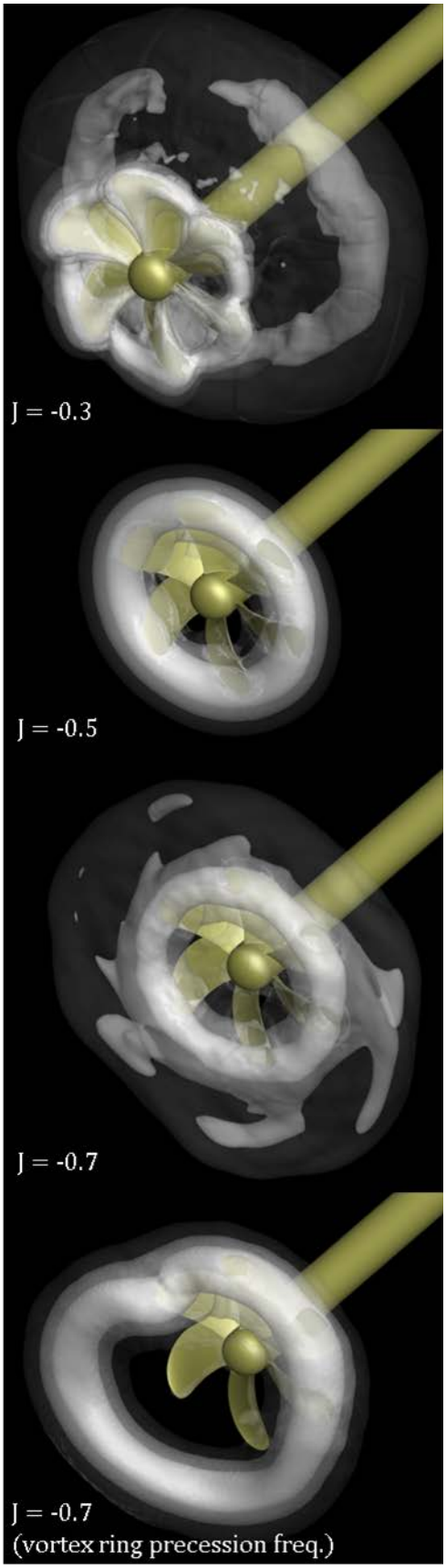

Figure 5: Phase-averaged pressure (average as described in Figure 4). Three iso-surfaces are shown for each case with increasing opacity: $-1\times, -2\times$ and $-4\times \rho U_0^2$.

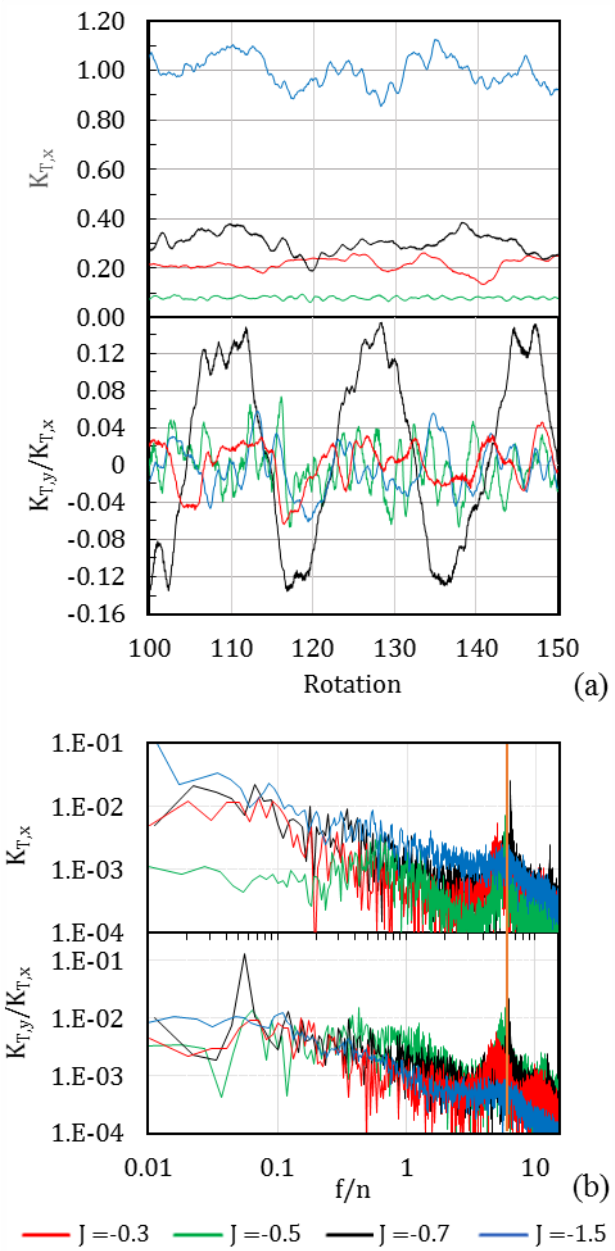

Figure 6: Longitudinal and lateral forces expressed as thrust coefficient; (a) time domain; (b) frequency domain.

Propeller forces, in the mean as shown in Figure 2 (OWC) and in the temporal and frequency domain (Figure 6), are also affected by the evolution of these coherent structures. A peak corresponding to the blade passage frequency is observed at all advance ratios, but its relative magnitude varies, with a maximum at intermediate J values. At low advance coefficients, below J = -0.5, the flow regime is characterized by high frequency instabilities, resulting from higher momentum input from the propeller producing a jet that travels upstream. As expected, a clear harmonic only exists at a frequency near the blade passage frequency as the blades hit the complex vertical structures generated by the highly turbulent flow. At the critical value of J = -0.5, the ring vortex is closest to the propeller plane. This stronger circulation has axially symmetric behavior, increasing the axial induced velocity and reducing the angle of attack with respect to conditions at lower and higher advance coefficients, producing a minimum in negative thrust. This was observed in experiments (Chesnakas et al., 2004) and LES simulations (Chang et al., 2008). Notice also both in the time and frequency domain the comparatively small magnitude of low frequency components, indicating that the slow variations associated with interaction of the free flow and the propeller induced flow are minimized at this condition. For J = -0.7 a second harmonic at about twice the blade passage frequency is also observed, as the rotating ring vortex typically touches more than one blade at the time. Finally, for J = -1.5 the blade passage frequency becomes less dominant, and instead a more uniform distribution for all frequencies is obtained, consistent with the more turbulent characteristics of the flow.

Shifts in the harmonic frequency with respect to the blade passage frequency are observed in Figure 6 for J = -0.3 (to lower values) and -0.7 (higher frequency). These changes appear to occur in relation to the direction of rotation of the ring vortex that changes from being co-rotating with the propeller for low advance ratio, to clearly counter-rotating for J = -0.7. The reason for the presence of a counter-rotating ring vortex at certain advance coefficients is still being investigated, but appears to be related to the distortion of the ring near the attachment point to the blade, which results in the alignment of vortex core with the longitudinal coordinate. This realignment is necessary to maintain closed vortical structures, as the more external portions of the vortex are advected downstream by the free-stream.

For more negative advance ratios, the effect of the ring vortex on thrust decreases as the distance to the propeller increases. The frequency observed is closest to the blade passage frequency for J = -0.5, which present the strongest and most stable vortex ring attached to the blade tips. The relation between vortex ring rotation and frequency shift is still not clear and continues to be a point of investigation.

Figure 6 also presents lateral forces for the same advance ratios previously described. Using components allows to identify the relationship between the lateral force and the presence of a rotating asymmetric ring vortex, as the maximum lateral force F_y (shown relative to thrust in Figure 6) coincides with the vortex being closest to the blades at y = 0, for intermediate values of the advance ratio (regime III in Figure 3). For J = -0.7 a low-frequency component, of period about 18 propeller rotations is observed; its frequency coincides with that of the rotation of the ring vortex. Similar results are observed for advance ratios in this regime, with ring vortex rotational period varying linearly from 16.4 propeller periods at J = -0.9 to 19.1 at J = -0.6. It is also observed that the amplitude of the oscillation, as extracted from the frequency domain analysis, increases linearly in this regime. For regime IV, as shedding of the vortex ring becomes more prevalent, the amplitude of the low-frequency peak associated with the ring vortex decreases rapidly. Finally this peak disappears completely in regime V. For moderate advance ratios, in

particular at J = -0.5, the strong symmetry of the flow reduces side forces to a minimum.

An alternative description of the side forces uses a resulting side force rather than the individual components,

$$K_S = \sqrt{K_{T,y}^2 + K_{T,z}^2} \quad (1)$$

This description has been used extensively in the literature (e.g., Chang et al., 2008; Jang and Mahesh, 2013). Figure 7 presents the resulting K_S for 7371R. Additionally, the amplitude associated to the ring vortex rotational frequency, as extracted from the Fourier analysis of the lateral force (indicated as $K_{y,RV}$ in Figure 7) is also shown. Figure 7 shows the relation between side forces and the presence of a ring vortex, as most of the contribution to K_S originate in the mode associated with the vortex ring. The contribution shown for transitional values J = -0.5 and -1 correspond to the predicted frequency for the ring vortex, as an extrapolation of the linear trend observed for the intermediate points. A smaller, less energetic peak is observed for J = -1 as the formation of a stable ring vortex is precluded by shedding. No relevant contribution is observed for J = -0.5. Peak values of side force, both absolute and as a fraction of K_T, are observed for intermediate advance ratios, approximately at J = -0.9 to -1.0. The regimes discussed previously are clearly observed here as well as J = -0.5 and -1 (regimes II and IV, respectively) represent transitions between the intermediate condition of a persistent ring vortex and the low and high advance coefficient regimes without a well-defined structure in the instantaneous flow.

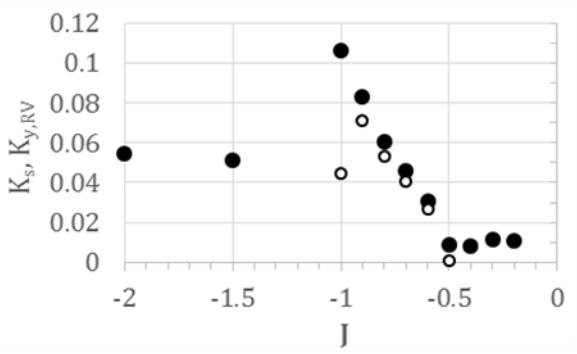

Figure 7: Side force coefficient (solid symbols) as defined in Equation (1); an equivalent coefficient for the amplitude of the Fourier mode associated with the ring vortex, $K_{y,RV}$ (open symbols), is also shown.

3.3 Submarine vehicle in crashback maneuver

A crashback maneuver was simulated for the Australian DSTO/MARIN Joubert BB2 design, fitted with a MARIN 7371R stock propeller, as part of an effort to characterize operation of submarines near the surface. Details on those simulations and comparison with experimental data for a free running model conducted at MARIN, in the Netherlands (Overpelt et al., 2015), are presented in Carrica et al. (2016). A crashback maneuver was used to stop a surfacing test and captured in the experimental campaign. While the highly unsteady nature of the crashback operation makes repeatability of this type of experiments very difficult, it was expected that the main features of the maneuver could be reproduced numerically.

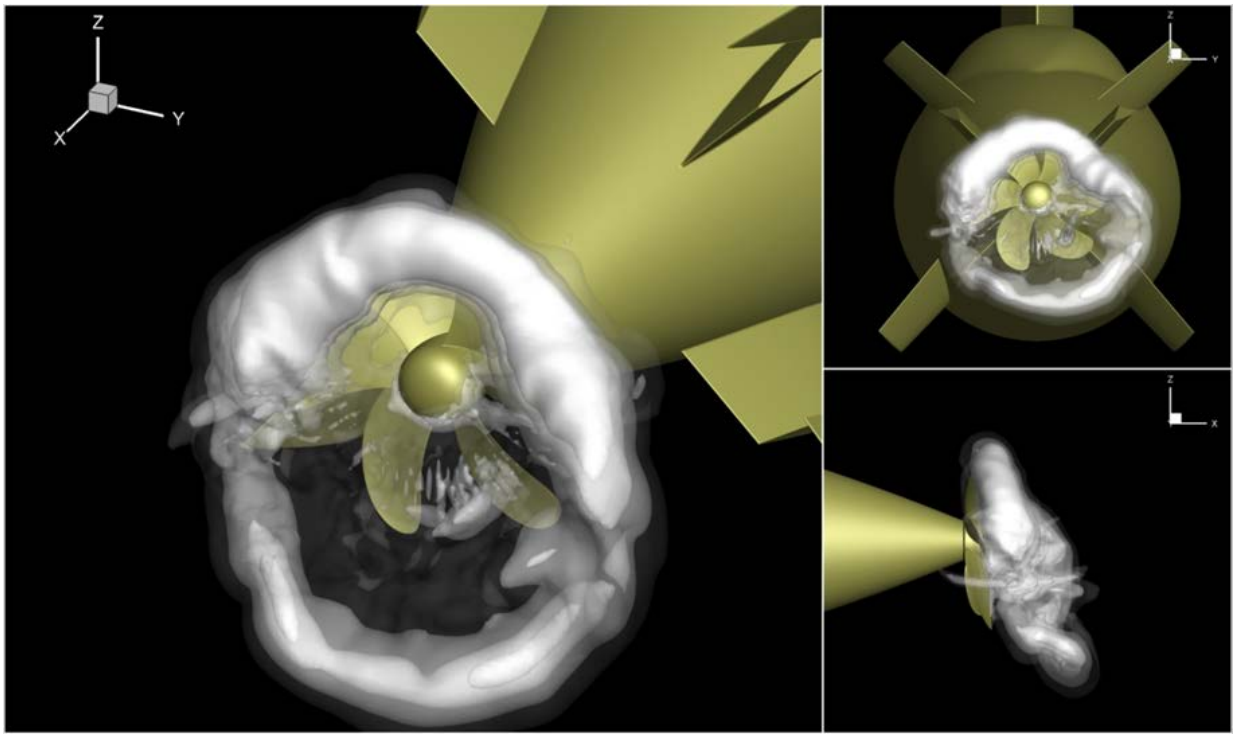

Figure 8: Instantaneous flow field for Joubert BB2 during a crashback maneuver. Three pressure iso-surfaces with increasing opacity identify the location of the ring vortex. The advance ratio is approximately J = -1.

In this case, the propeller rotational speed was reversed quickly and the submarine reacted by reducing forward speed, thus changing gradually from high negative advance coefficients to lower ones. Figure 8 shows the instantaneous flow at J = -1. An inclined, asymmetric ring vortex similar to those found in open water calculations is clearly observed. Figure 9 compares thrust for the experimental case and CFD results, showing overall good agreement between the two. Similar agreement is observed for torque (not shown). The largest discrepancies occur during the rapid transition from large negative advance ratios that correspond to the reversal of rotational direction of the propeller. Discrete points superimposed to the experimental curve at approximately 1 second intervals (model scale) illustrate the temporal evolution of the system. Uniform rotational speed is only established at J = -0.4, calculated with the vessel velocity. During the maneuver, pitch and yaw of the vessel varied from -5 to 15 and from 0 to about -10 degrees, respectively, and the presence of significant wakes from the submarine appendages (sail and rudders) produced very variable incoming flow conditions to the propeller; yet resulting forces are reasonably consistent with the calculated open water curves for 0 and 10 degrees of shaft inclination, also shown in Figure 9. Previous analysis of propeller performance during forward maneuvers (Martin et al., 2014) showed that differences between maneuver and open water operation occur mainly due to variations on the incoming flow to the propeller. In the case of a crashback it is apparent that the time scales associated with the formation of the recirculating flow around the propeller can be large compared to the fast change of flow conditions, and will also affect the operation of the propeller. Further work, possibly under more controlled conditions than those of a fully free running model are necessary to fully assess these effects.

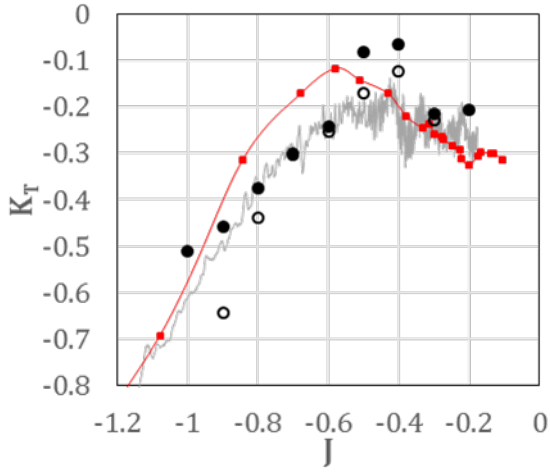

Figure 9: Thrust coefficient as a function of the advance ratio for Joubert BB2. Experimental measurements are shown in red with 1.07 s between reported values; CFD results are shown in grey, and OWC for 0 (solid symbols) and 10 degrees of shaft inclination (open) are also shown.

4 CONCLUSIONS

Numerical computations using the DDES-URANS solver REX were performed to analyze flow instabilities of two propellers operating in crashback. Good quantitative agreement with available data was observed, both in open water operation (for DTMB 4381) and during a free running maneuver of a submarine (for MARIN 7371R).

Analysis of the flow at different advance ratios in open water operation for 7371R allowed identifying several regimes, broadly characterized as an intermediate regime with a persistent, counter-rotating and asymmetric ring vortex responsible for the larges observed side forces; two transitional regimes, one at lower (absolute) advance ratios for which the ring vortex becomes symmetric and attached to the propeller and one at higher J for which the ring vortex becomes unstable and shedding occurs; and two extreme regimes occurring as continuations of these transitions, without persistent ring vortex structures in the instantaneous flow fields. The effect of these flow structures on the observed lateral forces, both in the mean and in the frequency domain was described.

Questions remaining and subject to on-going work include determining the mechanisms associated with the direction of rotation of the ring vortex for intermediate regimes (counter-rotating with respect to propeller and induced swirl direction); determining the relative stability of the different described regimes for different propellers, as for instance DTMB 4381 appears to present a much narrower region with a persistent asymmetric ring than 7371R; and providing a satisfactory description of the flow conditions leading to a marked loss of thrust at the transitional regime II.

5 Acknowledgements

This research was supported in part by the US Office of Naval Research under grant N000141410302, with Dr. Ki-Han Kim as the program manager. The computations were performed on computers at ERDC and Navy DoD Supercomputing Resource Centers.

REFERENCES

Bridges, D.H., Donnelly, M.J. & Park, J.T. (2008). 'Experimental investigation of the submarine crashback maneuver'. ASME. J. Fluids Eng., **130**, 011103-01-11.

Carrica, P.M., Kerkvliet M., Quadvlieg, F., Pontarelli, M., Martin, J.E. (2016). 'CFD Simulations and Experiments of a Maneuvering Generic Submarine and Prognosis for Simulation of Near Surface Operation'. Proceedings of the 31st Symposium on Naval Hydrodynamics, Monterey, CA, USA.

Chang P.A., Ebert M., Young, Y.L., Liu, Z., Mahesh K., Jang H., Shearer, M. (2008). 'Propeller forces and structural responses to crashback'. Proceedings of the 27th Symposium on Naval Hydrodynamics, Seoul, Korea, Vol. 2, pp. 1069–1091.

Chesnakas, C.J., Donnelly, M.J., Fry, D.J., Jessup, S.D., Park, J.T. (2004). 'Performance of Propeller 4381 in

Crashback'. NSWCCD-50-TR-2004/010. Naval Surface Warfare Center Carderock Division, West Bethesda, MD, USA.

Hecker, R., Remmers, K. (1971). 'Four quadrant open-water performance of propellers 3710, 4024, 4086, 4381, 4382, 4383, 4384 and 4426. Tech. Rep. NSRADC 417-H01, David Taylor Naval Ship Research and Development Center.

Jang H., Mahesh, K. (2013). 'Large eddy simulation of flow around a reverse rotating propeller'. J. Fluid Mech., **729**, pp. 151-179.

Jessup, S., Chesnakas, C., Fry, D., Donnelly, M., Black, S. Park, J. (2004). 'Propeller Performance at Extreme Off Design Conditions'. Proceedings of the 25th Symposium on Naval Hydrodynamics, St. John's, Canada.

Jiang, C.-W., Dong, R., Liu, H.-L., Chang, M.S. (1996). '24-inch water tunnel flow field measurements during propeller crashback'. Proceedings of the 21st Symposium on Naval Hydrodynamics, Trondheim, Norway.

Li, J., Castro, A.M., Carrica, P. M. (2015). 'A Pressure–Velocity Coupling Approach for High Void Fraction Free Surface Bubbly Flows in Overset Curvilinear Grids'. Int. J. Num. Meth. Fluids, **79**, pp. 343-369.

Martin, J.E., Michael, T.J., Carrica, P.M. (2014). 'Overset Simulations of a Submarine in Self-Propelled and Maneuvering Conditions'. Proceedings of the 30th Symposium on Naval Hydrodynamics, Hobart, Australia.

Menter, F.R. (1994). 'Two-Equation Eddy-Viscosity Turbulence Models for Engineering Applications'. AIAA Journal, **32**(8), pp. 1598-1605.

Overpelt, B., Nienhuis, B., Anderson, B. (2015). 'Free Running Manoeuvring Model Tests On A Modern Generic SSK Class Submarine (BB2)'. Pacific 2015, Sidney, Australia.